



Article

Kinetics of Austenite Formation in a Medium-Carbon, Low-Alloy Steel with an Initial Martensite Microstructure: Influence of Prior Austenite Grain Size

Navneeth Rajakrishnan ¹, Morteza Sadeghifar ^{1,*}, Pinaki Bhattacharjee ², Henri Champlaud ¹ 
and Mohammad Jahazi ¹ 

¹ Department of Mechanical Engineering, École de Technologie Supérieure, Montreal, QC H3C 1K3, Canada; navneeth.rajakrishnan.1@ens.etsmtl.ca (N.R.); henri.champlaud@etsmtl.ca (H.C.); mohammad.jahazi@etsmtl.ca (M.J.)

² Department of Materials Science and Metallurgical Engineering, Indian Institute of Technology Hyderabad, Kandi, Sangareddy 502285, Telengana, India; pinakib@msme.iith.ac.in

* Correspondence: morteza.sadeghifar@etsmtl.ca

Abstract: The impact of prior austenite grain size (PAGS) on the kinetics of austenite formation with an initial martensite microstructure was investigated in a medium-carbon, low-alloy steel. Two distinct PAGS of 117 and 330 μm , representing the range of grain sizes encountered in industries, were considered. In this analysis, high-resolution dilatometry was used to study the formation of austenite during continuous heating experiments. The analysis of the dilatometry results revealed that grain refinement accelerated the rate of austenite formation without impacting its austenite formation temperature. Intermittent quenching tests were conducted to elucidate the nucleation and growth mechanisms of austenite formation using a combination of optical, scanning electron microscopy (SEM), and electron backscatter diffraction (EBSD). The differences in austenite formation kinetics as a function of prior austenite grain size were quantified and modeled in the framework of diffusion-controlled nucleation and growth theories using the genetic algorithm optimization.



Academic Editor: Chao Yang

Received: 27 November 2024

Revised: 24 December 2024

Accepted: 30 December 2024

Published: 2 January 2025

Citation: Rajakrishnan, N.; Sadeghifar, M.; Bhattacharjee, P.; Champlaud, H.; Jahazi, M. Kinetics of Austenite Formation in a Medium-Carbon, Low-Alloy Steel with an Initial Martensite Microstructure: Influence of Prior Austenite Grain Size. *J. Manuf. Mater. Process.* **2025**, *9*, 10. <https://doi.org/10.3390/jmmp9010010>

Copyright: © 2025 by the authors. Licensee MDPI, Basel, Switzerland. This article is an open access article distributed under the terms and conditions of the Creative Commons Attribution (CC BY) license (<https://creativecommons.org/licenses/by/4.0/>).

Keywords: austenite; martensite; kinetics; mathematical model; phase transformation; prior austenite grains

1. Introduction

High-strength, medium-carbon, low-alloy steels are widely used in industrial products such as turbine shafts, landing gear, mold steel, etc. Most of these steels are manufactured through ingot casting, forging, and heat treatment. Heat treatment, often composed of a quenching and one or more tempering steps (Q&T), is a crucial stage that determines the final microstructures providing the mechanical properties of the final parts. Among various factors, the phase transformations occurring during heating (i.e., austenite formation) and cooling (i.e., martensite, bainite, or pearlite) play the most important role in determining the final mechanical properties of the material. While phase transformations during cooling have been extensively studied [1], recent advancements in high-strength steels have brought increased attention to microstructural changes during heating, particularly austenite formation [2]. Quantifying the impact of different microstructural constituents on the kinetics of austenite formation is of high interest from industrial as well as academic perspectives, in order to design more efficient and repeatable heat treatment processes, especially for high-value-added components such as aircraft landing gear. Specifically, for

such applications, a fully martensitic structure is needed at the end of the quenching step. However, due to the thickness of the part, the austenite grain size in the as-forged condition is not uniform from the surface to the center. Therefore, understanding how the kinetics of austenite formation is influenced by the initial grain size is crucial [3].

It is known that the austenite formation kinetics is affected by initial microstructural parameters such as the initial phase, grain size, and particle size. Dannoshita et al. [4] studied the impact of three different initial microstructures with initial ferrite–pearlite (P), bainite (B), and martensite (M) phases in a low-carbon steel. They found that during the inter-critical annealing, the kinetics of austenite formation varied with the initial phase. The isothermal holding at 740 °C demonstrated that the kinetics of austenite formation from initial ferrite–pearlite was quicker compared to that from the initial bainite microstructure, while the kinetics from initial martensite microstructure was the slowest among the three. The impact of the initial phase is apparent from the literature, which leads to the increase in studies on austenite formation from initial martensite microstructure [5–8].

The formation of secondary austenite from the initial martensite structure of a Fe-Ni-Mn alloy during heating was studied by Singh and Wayman [5]. They showed that the rate-controlling mechanisms were nucleation and growth through the long-range diffusional transformation. Wei et al. [6] studied the growth of austenite from the as-quenched martensitic microstructure in a low-carbon steel. They concluded that lath and packet boundaries were the most favorable nucleation sites for austenite formation. Shinozaki et al. [7] studied austenite formation of a Cr-Ni-Mo steel with a slow heating rate with an initial tempered martensite microstructure. They identified two types of austenite nucleation at lath boundaries, at prior austenite grains, and inside the grains. They also found that nucleation at lath boundaries formed acicular austenite grains and nucleation at prior austenite grain boundaries or inside grains formed globular austenite grains. The austenitization for 18NiCrMo5 steel with initial martensite structure was studied by Settimi et al. [8]. They reported a diffusive mechanism for low heating rates during austenite formation, whereas at high heating rates, the transformation was controlled by a displacive mechanism.

Mohsenzadeh et al. [9] described that in a steel with the initial microstructure of ferrite and cementite particles, the increase in the average ferrite grain size caused a decrease in the kinetics of austenite formation. For a medium-carbon, low-alloy steel, Fredj et al. [3] demonstrated that the nucleation rate increased with decreasing austenite grain size in an initial bainitic microstructure. Wang et al. [10] found that with the increase in the grain size in a nanostructured ferritic steel, both critical temperature and time taken for austenite formation increased. It is clear from the literature that the initial grain size plays a significant influence on the kinetics of austenite formation, but the studies considering the influence of the grain size did not address the phase transformation with initial martensite microstructure.

In recent years, there have been advancements in developing mathematical frameworks to analyze thermal processes associated with austenite formation, integrating thermodynamics with microstructural changes. The objective is to model treatment procedures accurately, employing kinetic models to predict the proportion of austenite. This approach aims to enhance precision in evaluating phase distribution within multiphase steel, particularly for designing microstructures.

The formation of austenite from ferrite–pearlite based initial microstructure has been modeled using Avrami, or Johnson–Mehl–Avrami–Kolmogorov (JMAK) [11–14]. Conventional models use thermodynamic equations to identify the kinetics parameters k and n [11,12]. The kinetics of austenite transformation from pearlite for a continuous heating and an isothermal transformation condition was studied by Garcia et al. [11] and Roos

et al. [12], respectively. Both groups used the Avrami equation to quantify the kinetics of austenite formation and expressed k and n as a function of nucleation and growth rates. In contrast, the determination of kinetics parameters with iteration, linear regression, or multiple regressions is based on experimental data, which were generally obtained through dilatometry [13,14]. Oliveira et al. [13] experimentally studied the kinetics of pearlite to austenite transformation in a low-carbon steel using different heating rates. They observed that the k value depends on the heating rate, while the n value is independent of the heating rate. Lopez-Martinez et al. [14] carried out a dilatometric analysis on the kinetics of austenite formation from bainite–martensite initial microstructure for heating rates less than 1 °C/s. They found that both kinetic parameters k and n increased with an increment in the heating rate. The authors explained the change in kinetics parameters with the change in growth mechanism during austenite formation. However, any of the above models did not directly consider the influence of prior austenite grain size of martensite before phase transformation.

The isothermal formation of austenite as a function of the grain size was modeled by Roosz et al. [12]. They reported that the nucleation rate was inversely proportional to the product of the average pearlite colony edge length with the square of the average true interlamellar spacing. Adopting the model developed by Roosz et al. [12] to suit continuous heating experiments, Caballero et al. [15] provided a mathematical model for the kinetics of non-isothermal ferrite–austenite transformation. They showed the Avrami equation can be used to successfully model the kinetics of the ferrite-to-austenite transformation.

The present research study aimed to investigate the kinetics of austenite formation of non-isothermal martensite–austenite transformation as a function of prior austenite grain size. Based on experimental results, a mathematical formulation was derived for this transformation kinetics by considering the nucleation sites and the growth of newly formed austenite grains. A combination of high-resolution dilatometry experiments, optical and electron microscopy, as well as EBSD was used for this investigation. In addition, mathematical modeling was conducted based on the fundamental mechanisms governing nucleation and growth on interfaces, and the kinetics parameters were calibrated with genetic algorithm optimization. There was excellent agreement between the mathematical model developed by modifying a ferrite model and the experimental results.

2. Methodology

In this section, first, the material and the parameters employed for the preparation of the initial martensite sample with different prior austenite grain sizes, dilatometry studies, intermittent quenching, and microstructural characterization are described. Then, the Genetic Algorithm method which was required to identify the kinetic parameters of the mathematical model defining the kinetics of austenite formation is explained.

2.1. Materials and Methods

The material studied in this work is a medium-carbon, low-alloy steel, with a nominal composition shown in Table 1. The material was provided by Finkl Steel-Sorel, Quebec, QC, Canada. Cylindrical samples with 10 mm in length and 4 mm in diameter were prepared for dilatometry experiments. The Bahr 805D/A high-resolution dilatometer (TA[®] Instruments, New Castle, DE, USA) was used to carry out the heat treatment for the preparation of initial microstructure, continuous heating dilatometry experiments, and intermittent quenching experiments.

In order to replicate different locations in an industrial size forged block, specific thermal cycles were selected to establish an initial microstructure characterized by a martensitic matrix with two distinct prior austenite grain sizes. The selected heating rate was set at

5 °C/s and the cooling rate at 10 °C/s, with two different isothermal holding durations of 5 and 240 min, as illustrated in Figure 1. The specimen subjected to a shorter isothermal holding time of 5 min exhibited smaller grain sizes (SG), while the sample with an extended isothermal holding time of 240 min displayed larger grain sizes (LG). The SG samples represent the grain sizes of the outer surface of the industrial size forged block and the LG samples represent those of the center.

Table 1. Chemical composition of medium-carbon, low-alloy steels in mass percentage.

C	Mn	Si	Ni	Cr	Mo
0.26	1.00	0.35	0.60	1.45	0.55

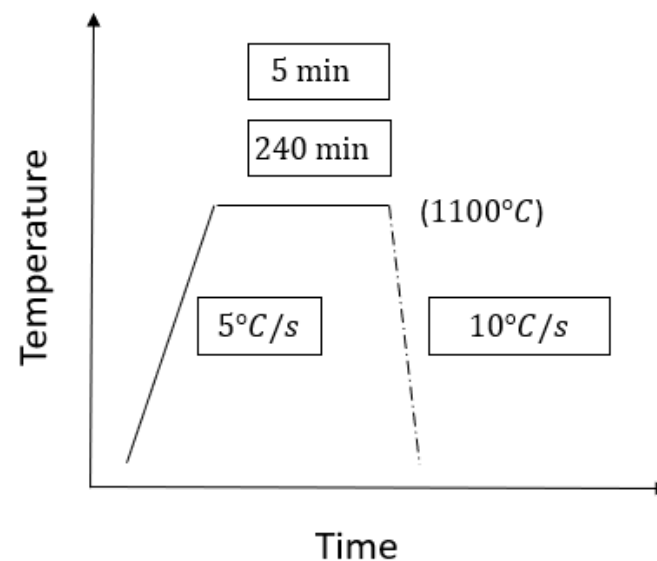


Figure 1. The thermal cycle with two different isothermal holding times for initial martensite formation.

The continuous heating experiments were conducted to analyze the kinetics of austenite formation at a heating rate of 5 °C/s for both the SG and LG samples. The austenite start and finish temperatures as well as its volume fraction in the inter-critical region were determined by dilatometric experiments [16].

To investigate the microstructure during austenite formation and gain insights into nucleation and growth mechanisms, samples were quenched from the inter-critical region, allowing the high-temperature austenite to transform into martensite at room temperature. This quenching process, referred to hereafter as intermittent quenching, facilitated the examination of the austenite at room temperature. The intermittent quenching tests were carried out subsequent to heating the samples above A_{c1} temperatures (780 and 790 °C) for the SG and LG samples, followed by immediate quenching using a helium gas. The heating rate employed was 5 °C/s, while the cooling rate was maintained at 40 °C/s.

The initial martensite microstructure and intermittent quenching microstructure were obtained by conventional chemical etching. Following the required heat treatment, the samples were prepared by grinding and polishing according to standard metallographic procedures. A chemical etchant, specifically 3% Nital, was utilized in the process to reveal the features of the martensitic microstructure. To study the influence of initial martensite microstructure, it is essential to quantitatively measure the microstructure by revealing the prior austenite grains. Although etchants such as Nital, Vilella, and other picric acid-based solutions with wetting agents are commonly used to reveal prior austenite grains, they were not effective in this study. Empirical evidence from the literature indicates that chemical etching is generally unsuccessful in revealing prior austenite grain boundaries in low-

and medium-carbon steels [17]. This may be due to the negligible difference in chemical composition between the prior austenite grain boundaries and the matrix.

The thermal etching technique was therefore employed to reveal the prior austenite grains [17]. Initially, the as-received samples underwent standard metallographic procedures, including grinding and polishing. Subsequently, the as-polished samples were subjected to a heat treatment cycle that replicated the conditions of austenite formation in both the SG and LG samples. Thermal etching reveals prior austenite grain boundaries by creating grooves at their intersections with a polished surface. This technique involves heating a pre-polished sample in an inert atmosphere. The resulting grooves make the boundaries visible under a light optical microscope at room temperature. This technique shows the austenite grains which were formed during the thermal simulation of the required heat cycle. The heat cycle used is the same as the one used for the preparation of the SG and LG samples. To find the PAGS of the SG sample, the sample was heated at 5 °C/s up to 1100 °C and held at 1100 °C for 5 min before cooling down. For revealing the PAGS of the LG sample, the sample was heated at 5 °C/s up to 1100 °C and held at 1100 °C for 240 min before cooling down. The thermal etching technique helped quantify prior austenite grains [17]. The prior austenite grain size of both the SG and LG samples was measured from the microstructure obtained by thermal etching, employing an ASTM E-112 standard method.

The laser confocal microscope LEXT4100 (Olympus®, Tokyo, Japan), a light optical microscope was used in this study to analyze the microstructure after chemical etching and thermal etching. The microstructure after intermittent quenching was further analyzed by the SEM-EBSD technique using the SU8230 Hitachi Field-Emission Gun Scanning Electron Microscope (Hitachi, Tokyo, Japan) equipped with Bruker FlatQuad detector. For the EBSD investigation, the samples were prepared using ion milling on a Hitachi IM4000-plus ion miller machine (Hitachi, Tokyo, Japan). Data acquisition was performed at an operating voltage of 25 kV, a working distance of 18 mm, and a step size of 0.16 µm. The post-processing of EBSD data was conducted using the ESPRIT 2.2 software.

2.2. Genetic Algorithms

Genetic Algorithm (GA) is a technique used for solving optimization problems. GA searches the design space based on random number generations using natural selection. GA is versatile and can be applied to various optimization challenges, particularly those where the objective function is discontinuous, non-differentiable, stochastic, or highly nonlinear. It differs from classical, derivative-based optimization algorithms. The following outline summarizes how GA works [18,19].

(i) The algorithm begins by generating a random initial population. Each population consists of an array of individuals, also known as chromosomes, genomes, or strings. Each individual is represented as a vector with entries referred to as genes, which are the design variables in the optimization process.

(ii) The algorithm then generates a sequence of new populations. In each generation, the GA selects individuals with better fitness values from the current population, known as parents, to produce the next population, referred to as children. Three types of children are created:

- (a) Elite children: These are selected from the individuals in the current population with the highest fitness values. These elite individuals automatically survive to the next population. This process is known as reproduction.
- (b) Crossover children: These are created by combining the genes of a pair of parents. This operation, known as crossover, is typically applied with a high probability.

- (c) Mutation children: These are generated by applying random changes to a single parent. This operation, known as mutation, is applied with a low probability and helps prevent the GA from getting stuck in local minima.

The algorithm replaces the current population with the children to create the new population.

(iii) The algorithm stops once the stopping criterion is met.

Moreover, some important terminology in GA is defined as follows:

“Population size” refers to the number of individuals present in each generation.

“Elite count” specifies the number of individuals guaranteed to survive to the next generation.

“Crossover fraction” specifies the fraction of the next generation, excluding elite individuals, that are generated by crossover. The remaining individuals in the next generation are produced by mutation.

“Function tolerance” refers to the threshold value. If the cumulative change in the fitness function value is less than this tolerance, the algorithm stops.

The mathematical model in this study that describes the kinetics of phase transformation for martensite-to-austenite transformation needed an optimization technique to identify the kinetic parameters based on the experimental results. The GA described in this section was instrumental in identifying the coefficients of kinetics parameters. In the following sections, details on how the GA was applied to determine the coefficients of kinetics parameters were described.

3. Results and Discussions

3.1. Initial Microstructure

The SG and LG initial martensite microstructures were analyzed with the optical images shown in Figure 2. The microstructure obtained has a lath martensite microstructure with no apparent grain boundaries as seen after conventional etching. Figure 3 shows the microstructure with prior austenite grains revealed by thermal etching of the SG and LG samples. The SG sample has a prior austenite grain size (PAGS) of $117\mu\text{m}$, and the LG sample has a PAGS of $330\mu\text{m}$. The thermal etching technique successfully simulated the required microstructure to obtain PAGS that could not be revealed by chemical etching.

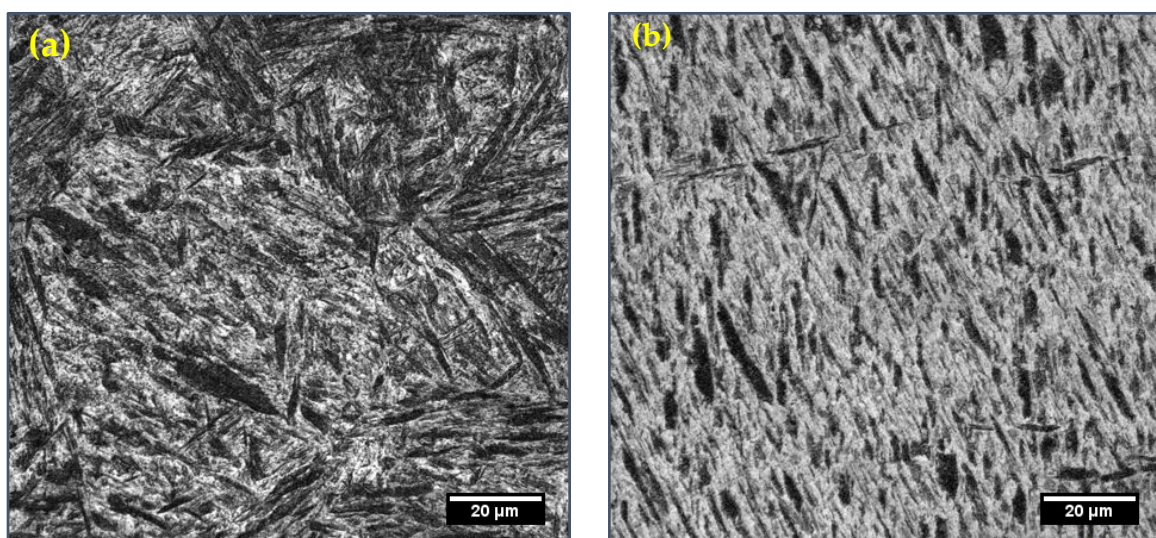


Figure 2. Initial martensite microstructure with (a) 5-min isothermal holding and (b) 240-min isothermal holding.

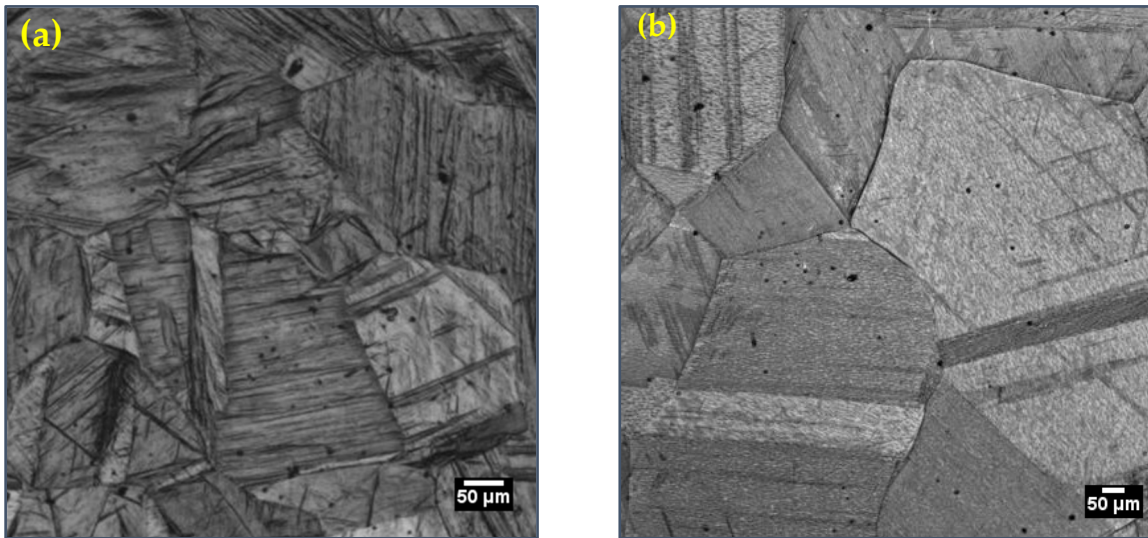


Figure 3. Thermal etching revealing prior austenite grain for (a) 5-min isothermal holding at 1100 °C and (b) 240-min isothermal holding at 1100 °C.

3.2. Kinetics of Austenite Formation

Continuous heating experiments were carried out using the dilatometer to study the impact of PAGS on the kinetics of austenite formation. The thermal cycle used to prepare samples with two different grain sizes was designed in such a way that the SG samples had grain sizes close to that of the surface and the LG sample had grain sizes close to that of the center of a 40 metric ton forged ingot. Therefore, the difference in kinetics between the SG and LG samples shows the difference in the kinetics of austenite formation in different parts of the forged ingot. The dilatometry curves of the SG and LG samples with a heating rate of 5 °C/s are shown in Figure 4. The austenite start and finish temperatures were identified from the dilatometric curves. The beginning of contraction from the linear expansion marks the austenite start temperature and the end point of contraction that joins back to the linear expansion is the austenite finish temperature.

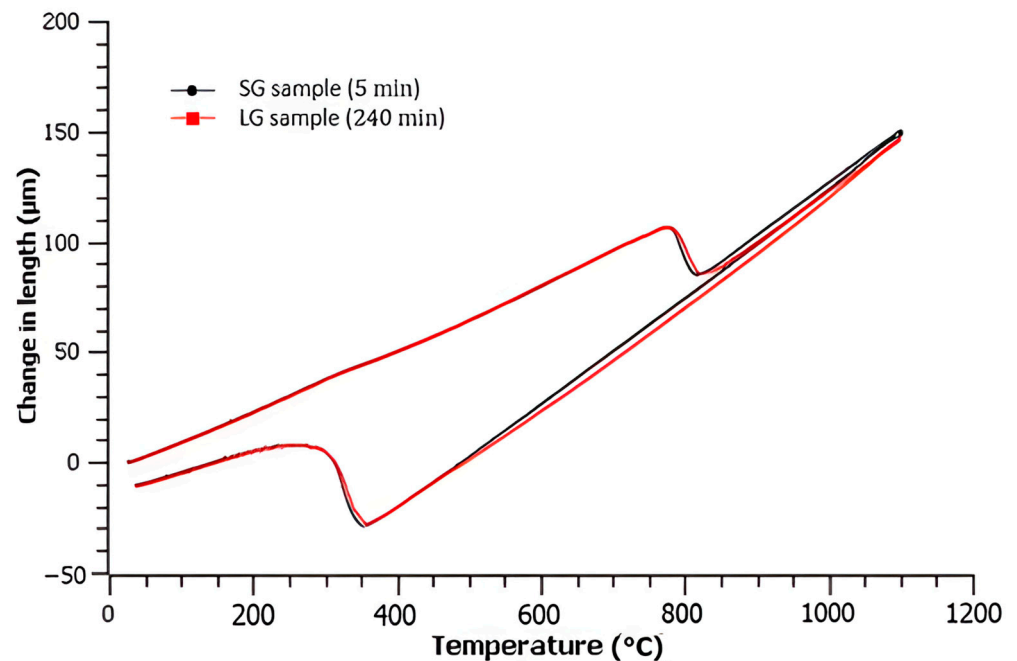


Figure 4. The dilatometry curves of the SG and LG samples.

Table 2 shows the values of the start and finish temperatures of both samples for a heating rate of 5 °C/s. As seen in this table, there are no changes in austenite start temperatures with the change in PAGS of the initial martensite microstructure. These findings are in contrast with those of Wang et al. [10], who observed that the onset temperature of austenite formation (A_{c1}) was increased with increasing the grain size in a nanostructured ferritic steel. The mechanically induced nanostructures have interfaces with high stored energy. The difference in stored energy because of changes in the grain size leads to an increase in critical temperature with an increase in the grain size. The SG and LG samples in annealed conditions with an insignificant difference in stored energy do not show the variation in critical temperature with the change in initial grain size.

Table 2. The critical temperature of the SG and LG samples heating at 5 °C/s.

Transformation Temperature (°C)	SG	LG
Start temperature	756	756
End temperature	820	816

Figure 5a shows the evolution of the volume fraction of austenite with time as a function of the grain size. The lever rule was applied to the dilatometry results at inter-critical temperatures to calculate the volume fraction of austenite. The results show that the SG samples, whose grains were finer, have faster kinetics than the LG samples with larger grains. The samples exhibit kinetic behavior depicted by an S-shaped sigmoidal curve. Initially, the transformation proceeds slowly, until the formation of 10% austenite. Then, the growth accelerates rapidly until reaching 95% austenite. This rapid growth, evident in the linear middle segment of the sigmoidal curve, highlights the distinction between the SG and LG samples. As temperature rises, both the driving force for phase transformation and diffusion increase, leading to an accelerated growth. The transformation rate (volume fraction of austenite formed with respect to time) eventually reaches a plateau, indicating the completion of the phase transformation. Figure 5b shows the difference between the rate of austenite formation for the SG and LG samples. It can be seen that the transformation rate of the SG sample is always higher than that of the LG sample. The peak difference occurred at 8 s, showing about a 20% difference in the volume fraction of austenite formed between the SG and LG samples.

3.3. Intermittent Quenching

It is well known that the nucleation and growth mechanisms are responsible for austenite formation during heating [20–22]. The influence of nucleation and growth on the kinetics of austenite formation based on PAGS was analyzed with the help of the microstructures obtained from intermittent quenching. It is essential to know the nucleation sites for austenite formation to understand and quantify the kinetics of phase transformation. In the present work, intermittent quenching was performed at 780 °C and 790 °C for the SG samples and 780 °C for the LG samples in the inter-critical range to reveal the nucleation sites and growth of newly formed austenite grains.

Figure 6 shows the nucleation site of austenite on the SG and LG samples. The white region seen in the microstructure is high-temperature austenite that converted to martensite [12]. Figure 6a illustrates that austenite is nucleated on prior austenite grains for the SG sample. Figure 6b displays after quenching at 780 °C, not only did the majority of the nucleation happen on the prior austenite grain boundaries in the LG samples, but there are also white spots that represent austenite nucleation inside the grains, in addition to those at the grain boundaries. Figure 6c demonstrates nucleation inside the grains for the SG samples at 790 °C.

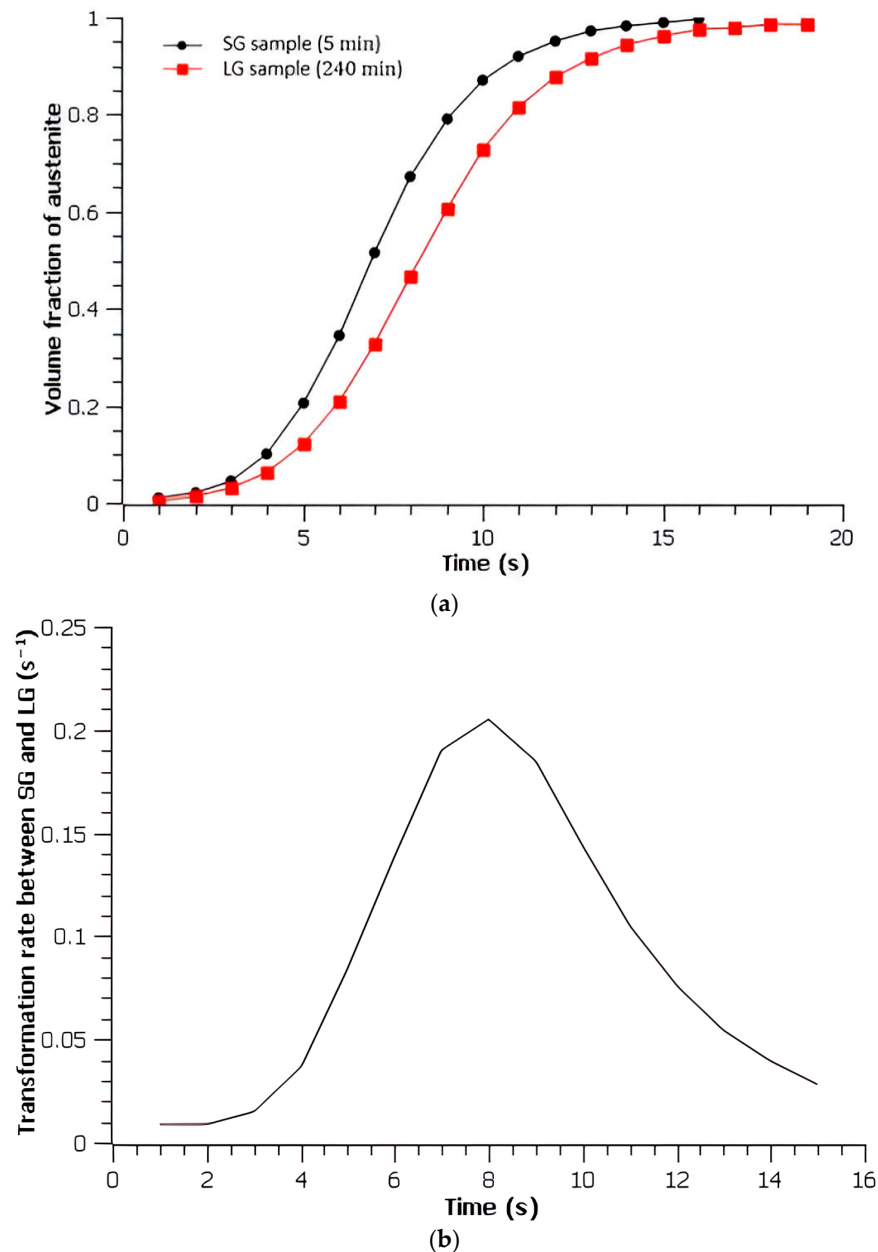


Figure 5. (a) Kinetics of austenite formation for SG (5 min) and LG (240 min) samples and (b) the transformation rate for the SG and LG samples.

The above results indicate that at the beginning of the transformation, the preferential austenite nucleation site on martensite is at the prior austenite grain boundary. At higher temperatures, after site saturation on the prior austenite grain boundary, the secondary preferential nucleation site becomes activated inside the grains. No experimental report is available on austenite nucleation sites in an initial martensite structure; however, the above findings are in agreement with those of Speich et al. [23], who also reported that additional nucleation sites became activated as the phase transformation progressed in an initial pearlitic microstructure. In addition, they observed that nucleation occurred in pearlite colonies at temperatures just above A_{c1} and as the temperature increased, nucleation sites were found at the ferrite-ferrite interface [23].

The EBSD analysis after intermittent quenching allowed us to identify the difference between the nucleation of the SG and the LG samples. The dark regions (non-indexed) on the band contrast images demonstrate the nucleation sites on grain boundaries [24]. As

the indexing of martensite (indicative of high-temperature austenite) is less because of the inherent strain in the microstructure, the martensite appeared as non-indexed regions in Figure 7. The Inverse Pole Figure (IPF) maps are depicted in Figure 8. It can be seen that the SG sample has austenite growth seen as non-indexed regions, whereas the LG samples show growth seen as indexed regions. The IPF maps and band contrast images reveal that the strain energy associated with the nucleation of austenite is different between the SG and LG samples. It underlines the difference in nucleation pattern for the change in prior austenite grain size. Therefore, separate equations were formulated for each grain size.

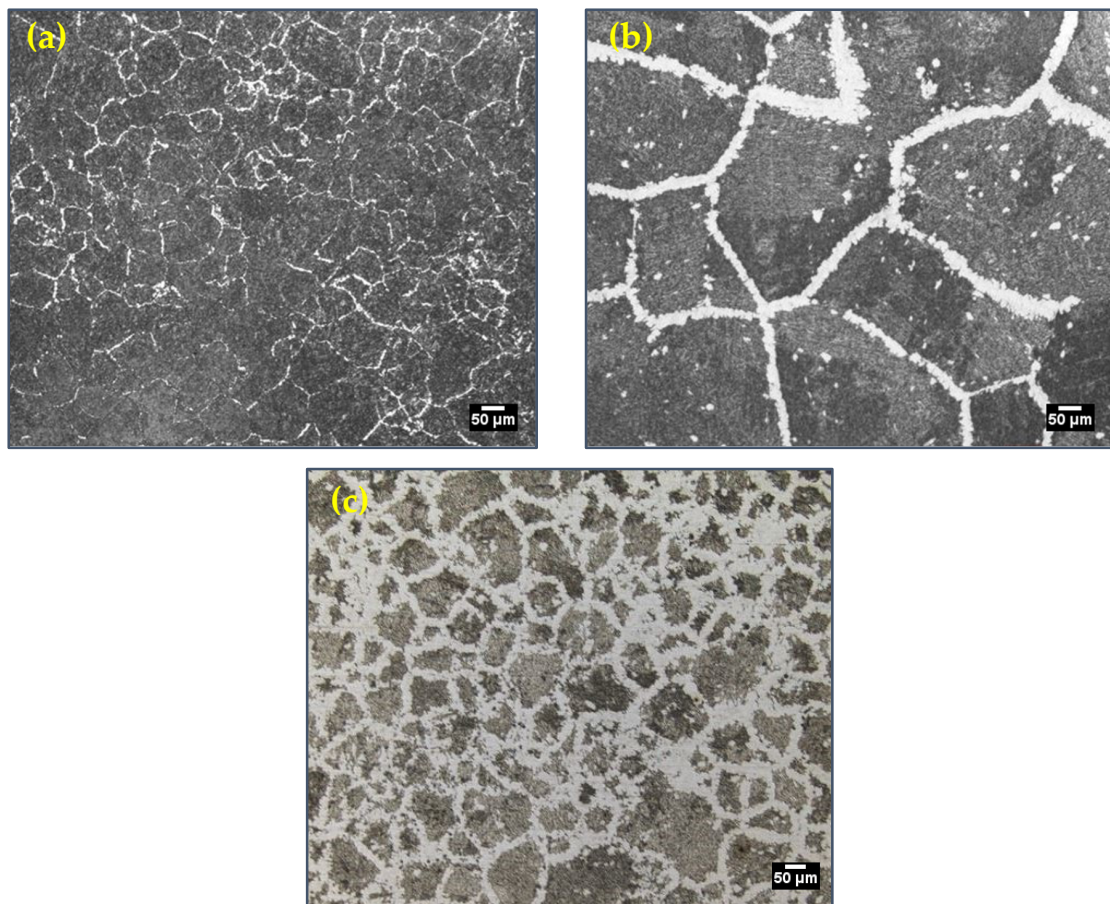


Figure 6. (a) The SG sample quenched at 780 °C, (b) the LG sample quenched at 780 °C, and (c) the SG sample quenched at 790 °C.

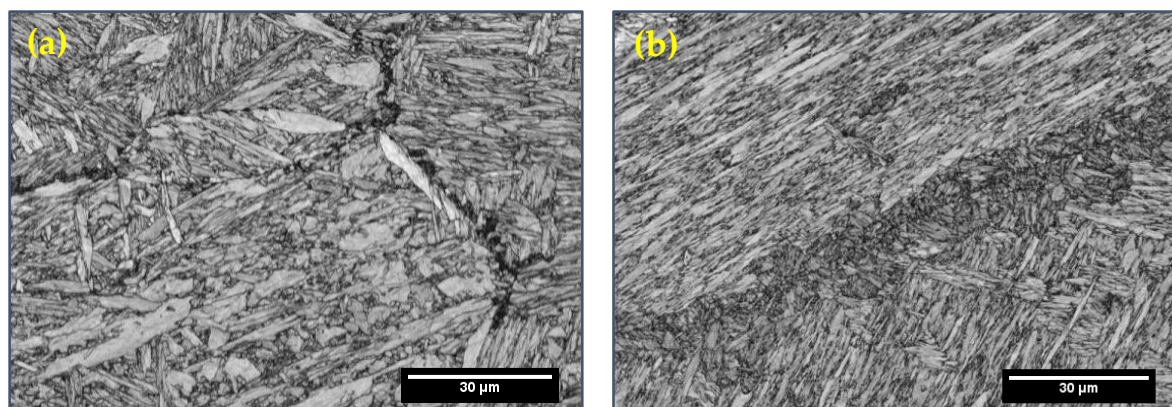


Figure 7. Band contrast image for (a) the SG sample and (b) the LG sample, showing austenite formation at grain boundaries.

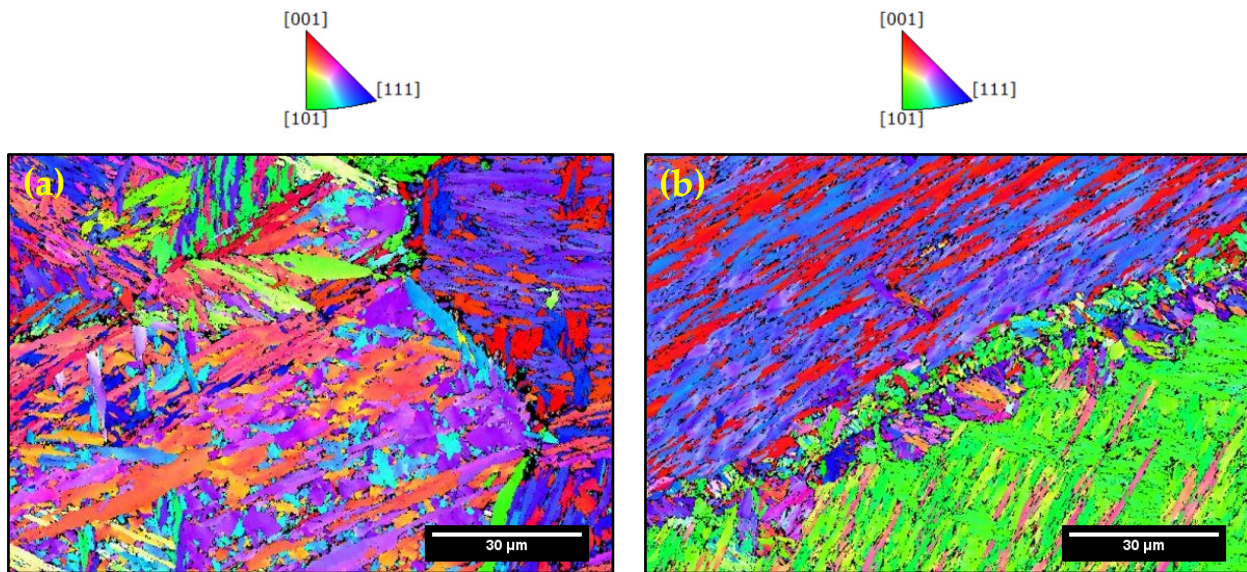


Figure 8. IPF maps for (a) the SG sample and (b) the LG sample, showing austenite formation at grain boundaries.

3.4. Mathematical Modeling

A mathematical model of the martensite-to-austenite transformation with the influence of an initial microstructure is presented in this section. As mentioned above, Caballero et al. [15] proposed a mathematical model describing the non-isothermal ferrite–austenite transformation. They assumed nucleation at α/α grain boundaries and the nucleation sites on grain boundary faces, edges, and corners, all of which were considered as potential nucleation sites in their model. They also assumed that site saturation occurred during nucleation and the transformation was controlled by the growth.

In the present work, the above model was modified to incorporate all the potential nucleation sites on the grain boundary. It must be noted that, based on the results reported in Figure 6, it was also assumed that new austenite grains mainly formed at prior austenite grain boundaries. Cahn [25] reported that when the nucleation occurs at the grain boundary at high nucleation rates, which is the case during the transformation of martensite to austenite, site saturation occurs, and the kinetics is controlled by the growth rate.

The growth rate can be calculated by the absolute reaction rate theory [26]. The growth is an interface-controlled process, and the growth rate G is given by:

$$G = \frac{\delta\vartheta}{kT} \exp\left(\frac{-\Delta G_{act}}{kT}\right) \Delta g^{\alpha \rightarrow \gamma} \quad (1)$$

$$G = \frac{\delta\vartheta}{kT} \exp\left(-\frac{\Delta S}{k}\right) \exp\left(-\frac{\Delta H}{kT}\right) \Delta g^{\alpha \rightarrow \gamma} \quad (2)$$

where δ is the boundary thickness equal to 0.5 nm [15], ϑ is the number of attempts to jump the boundary activation barrier per unit time, k is the Boltzmann constant, T is the absolute temperature, ΔG_{act} is the free energy for the activated transfer of atoms across the martensite/austenite interface, ΔS is the entropy of activation per atom, ΔH is the enthalpy of activation per atom, and $\Delta g^{\alpha \rightarrow \gamma}$ is the Gibbs free energy difference per atom between the martensite and austenite phases. The value of ΔH is widely assumed to be equal to the enthalpy of activation for grain boundary diffusion [27] and has been reported to be between -232×10^{-21} and -277×10^{-21} J/atom [23].

In the present work, a ΔH value of -240×10^{-21} J/atom was determined to be suitable for both SG and LG samples. The assumed ΔH value is comparable to that of the ΔH

values used in the literature [27]. The frequency of atomic jump ϑ is equal to kT/h , where h is Planck's constant. As reported in Table 2, the temperature at which austenite formation occurs is 1027 K. At this temperature, the value of ϑ was calculated to be $1.9 \times 10^{13} \text{ s}^{-1}$.

The thermodynamic software package Thermo-Calc 2022b was utilized to compute the ΔS and $\Delta g^{\alpha \rightarrow \gamma}$. The graphical mode of Thermo-Calc was employed for this purpose. The database TCFE9 (steels: Fe alloys version 9.30) was used. The composition, as mentioned in Table 1, was specified in the system definer as input data. The difference in the entropy value between austenite formation temperature and room temperature gives the entropy of activation. The ΔS calculated is $7 \times 10^{-23} \text{ J/atom}$.

The Gibbs free energy change for the BCC-FCC transformation $\Delta g^{\alpha \rightarrow \gamma}$ was calculated using the Thermo-Calc software. Figure 9 shows the variation in $\Delta g^{\alpha \rightarrow \gamma}$ as a function of temperature. It can be seen that with an increase in temperature, the difference in the Gibbs free energy between the BCC and FCC phases diminishes, indicating a rise in the stability of austenite and a reduction in the stability of the BCC phase. The $\Delta g^{\alpha \rightarrow \gamma}$ as a function of temperature was also calculated for ARMCO steel using the same technique and the values were compared with those in the literature [15]. The values of $\Delta g^{\alpha \rightarrow \gamma}$ as a function of temperature from Thermo-Calc are in good agreement with those in the literature, showing the reliability of the calculation technique used in this research.

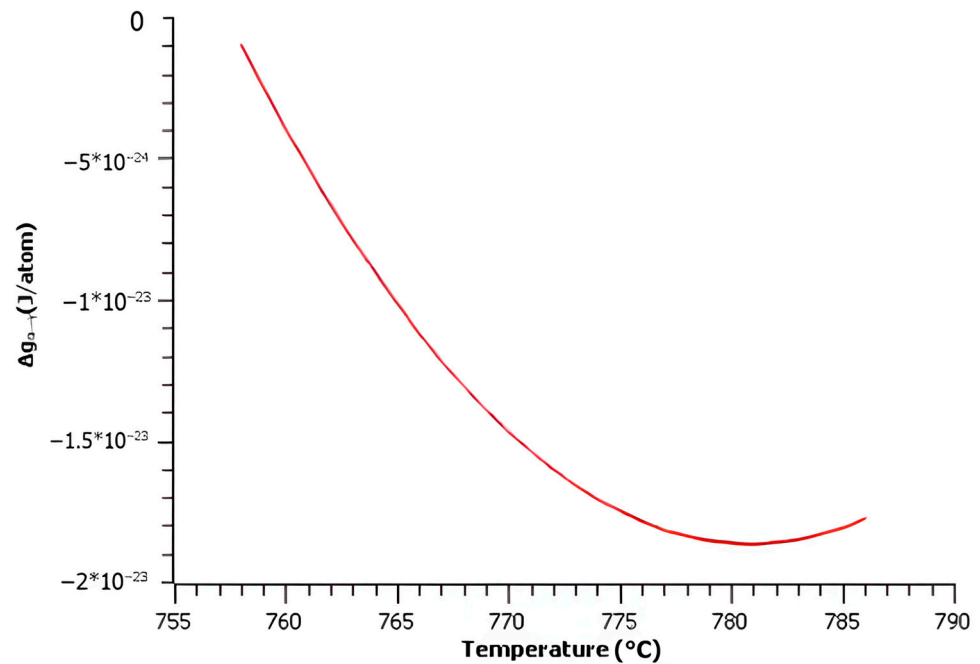


Figure 9. Gibbs free energy difference per atom between the BCC and FCC phases calculated using Thermo-Calc.

The Gibbs energy value is expressed as a quadratic equation by fitting the obtained curve shown in Figure 9 as:

$$\Delta g^{\alpha \rightarrow \gamma} = \left(-3.7 \times 10^{-20} + 8.38 \times 10^{-21}T + 9.6 \times 10^{-22}T^2 \right) \tag{3}$$

By inserting Equation (3) into Equation (2), the growth rate is calculated as:

$$G = \frac{85}{kT} \left(-3.7 \times 10^{-20} + 8.38 \times 10^{-21}T + 9.6 \times 10^{-22}T^2 \right) \exp \left(-\frac{-240 \times 10^{-21}}{kT} \right) \tag{4}$$

The Avrami equation for growth kinetics with site saturation and three activated growth sites at grain boundary edges, grain boundary faces, and grain boundary corners can be expressed as [25]:

$$V_\gamma = 1 - \exp[-(k_s t + k_e t^2 + k_c t^3)] \tag{5}$$

where V_γ represents the austenite volume fraction formed, t is the time, and k_s , k_e , and k_c are given by:

$$k_s = 2G \frac{S}{V}, k_e = \pi G^2 \frac{L}{V}, K_c = \frac{4}{3} \pi G^3 \frac{C}{V} \tag{6}$$

in which $\frac{S}{V}$, $\frac{L}{V}$, and $\frac{C}{V}$, respectively, are the boundary area, the edge length, and the grain corner number, all of which are per unit volume.

The model also has to incorporate the prior austenite grain size. The ferrite model by Caballero et al. [15] assumes that grains have a tetrakaidecahedra shape (i.e., a polyhedra with 14 faces). The same consideration is made in the present work based on the assumption that the nucleation sites are at grain boundaries from an equiaxed microstructure. The grains shaped like tetrakaidecahedra can effectively define nucleation sites at grain boundaries based on the grain size. Therefore, the assumption holds true. All grains are equally sized tetrakaidecahedra and they fill space such that square faces are (100) planes and hexagonal faces correspond to (111) planes.

$$\left. \begin{aligned} \frac{S}{V} &= \frac{3.35}{D} \\ \frac{L}{V} &= \frac{8.5}{D^2} \\ \frac{C}{V} &= \frac{12}{D^3} \end{aligned} \right\} \tag{7}$$

And hence,

$$\left. \begin{aligned} k_s &= \frac{6.7G}{D} \\ k_e &= \frac{26.7G^2}{D^2} \\ k_c &= \frac{50.3G^3}{D^3} \end{aligned} \right\} \tag{8}$$

in which G is given in Equation (4).

To address this equation for the non-isothermal reaction, the growth rate is expressed in terms of the assembly's state rather than the thermal path. Therefore, the time t is expressed as a function of temperature and heating rate, and the volume fraction is integrated over the given temperature, eventually yielding the equation for the volume fraction of austenite formed as:

$$V_\gamma = 1 - \exp \left\{ - \int_{T_s}^T \left[\frac{6.7}{\dot{T}D} G + \frac{53.4}{(\dot{T}D)^2} G^2 (T - T_s) + \frac{150.8}{(\dot{T}D)^3} G^3 (T - T_s)^2 \right] dT \right\} \tag{9}$$

$$V_\gamma = 1 - \exp \left\{ - \int_{T_s}^T \left[\frac{A}{\dot{T}D} G + \frac{B}{(\dot{T}D)^2} G^2 (T - T_s) + \frac{C}{(\dot{T}D)^3} G^3 (T - T_s)^2 \right] dT \right\} \tag{10}$$

The coefficients of the three activated growth sites are expected to be different for the SG and LG samples as their nucleation patterns are different. As a result, the coefficients of the three activated growth sites were replaced with variables A , B , and C , as shown in Equation (10). As seen in literature, the functional dependence of nucleation rate on grain boundaries, edges, and corners are constant while the coefficients were taken as approximate values [25]. In this study, the coefficients were optimized using the least squares optimization technique implemented with genetic algorithms, as detailed below.

3.5. Optimal Design of the Mathematical Model

To obtain a mathematical model best fitted to the experimental data of the volume fraction of austenite for the SG and LG samples, it is required to find the optimal values of A , B , and C .

The objective function was coded, and the optimization process was performed using the genetic algorithm (GA) solver provided in MATLAB® R2020b. The optimization problem was formulated as:

$$\text{Find } A, B, \text{ and } C \text{ to Minimize } \sum (V_{\gamma,Exp} - V_{\gamma})^2 \tag{11}$$

where A , B , and C are the design variables (see Table 3 for the GA results), and $V_{\gamma,Exp}$ and V_{γ} are the volume fraction of austenite at different temperatures from A_{c1} to A_{c3} measured in the experiments and modeled in the mathematical modeling (Equation (10)), respectively. In addition, $\sum (V_{\gamma,Exp} - V_{\gamma})^2$ is the objective function defined based on the least squares technique (LST).

Table 3. Coefficients of three activated growth sites calculated using the GA.

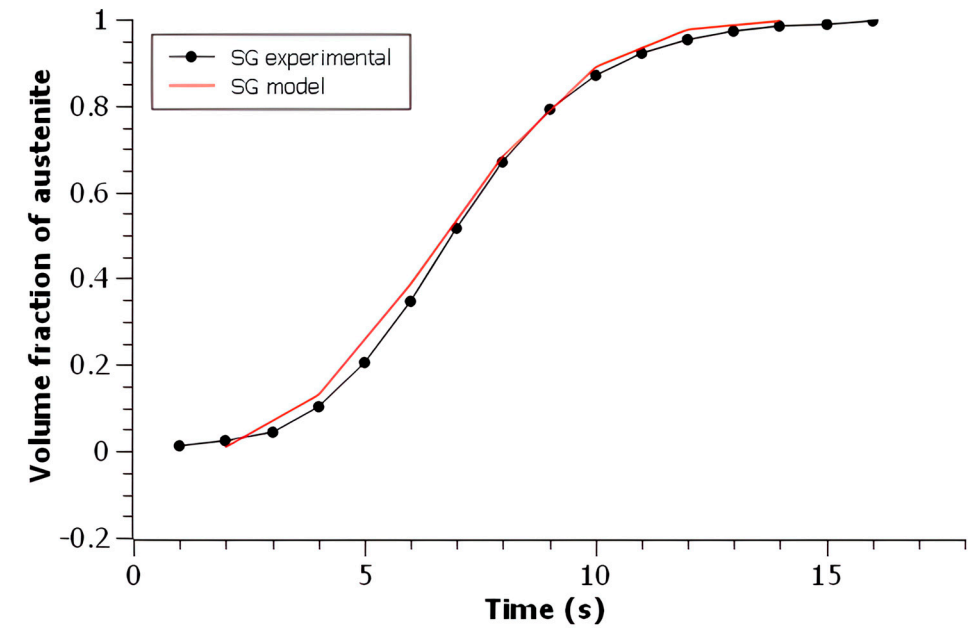
Grain Size (μm)	Coefficients of Activated Growth Site		
	A	B	C
330	1	74.1	73.4
117	0.48	13.3	4

It is required to explore a range of values for the GA elements to capture the most accurate optimum value. As a result, based on the user experience and the instructions in the GA user manual in MATLAB®, various values of “Population Size” ranging from 50 to 400, “Crossover Fraction” from 0.70 to 0.90, and “Elite Count” from 2 to 20, were explored in the GA optimization tool. Furthermore, the number of “Generations”, “Stall Generations”, and “Function Tolerance” were set as stopping criteria in the GA tool to 500, 50, and 1×10^6 , respectively. The optimum values of A , B , and C for each grain size are reported in Table 3. The calculated volume fraction using the mathematical model is plotted and compared with the experimental values, as shown in Figure 10.

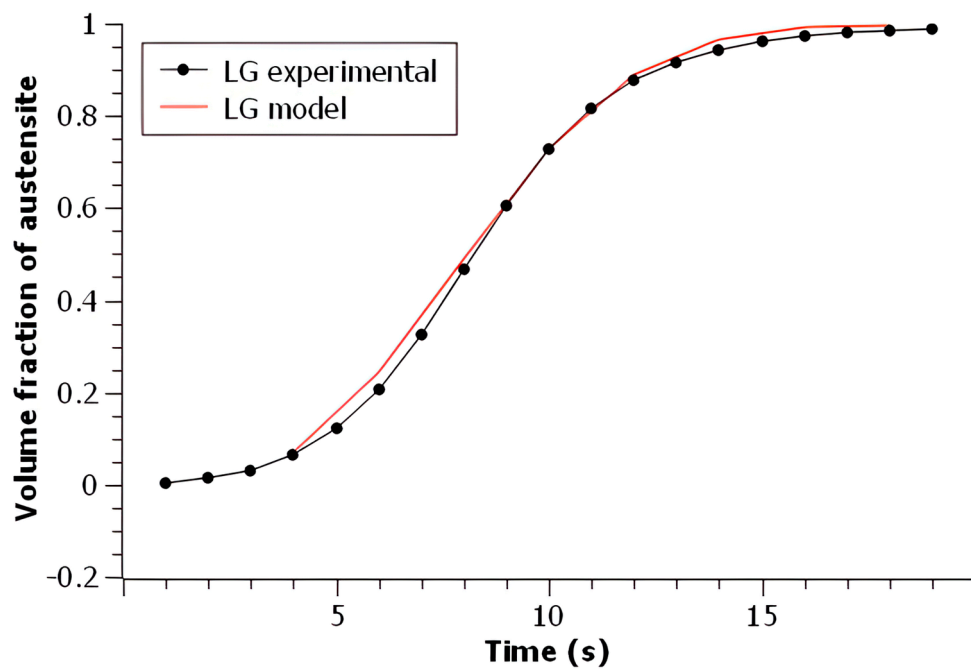
The R^2 value of both predictive mathematical models is 0.99, demonstrating very good agreement between the mathematical model and the experimental results. The experiment and model for the LG sample differ in the first two seconds of the transformation.

The model considers that rapid nucleation and growth rates control the kinetics of austenite formation. The LG sample exhibits a lower nucleation rate compared to the SG sample due to a smaller prior austenite grain boundary area, which acts as a nucleation site. This lower nucleation rate could explain the discrepancy between the modeling and experimental values for the first two seconds in the LG sample.

The mathematical model developed by Caballero et al. [15] for the ferrite-to-austenite phase transformation was successfully adapted in this study to examine the impact of initial grain size on the martensite-to-austenite phase transformation. The frequency value of atomic jump θ , the enthalpy of activation per atom ΔH , and the entropy of activation per atom ΔS were adjusted to account for the specific material used in this study. The Gibbs free energy change per atom was calculated using Thermo-Calc and expressed as a quadratic function of temperature. Finally, the kinetic parameters A , B , and C in Equation (10), representing nucleations at grain boundaries, grain edges, and grain corners, respectively, were modified for each grain size using the least squares optimization technique with a genetic algorithm solver.



(a)



(b)

Figure 10. Comparison of modeled and measured kinetics of austenite formations for (a) the SG sample and (b) the LG sample.

4. Conclusions

In the present work, the influence of PAGS on the kinetics of austenite formation has been investigated for a medium-carbon, low-alloy steel. The following conclusions can be drawn:

1. The kinetics of austenite formation from an initial martensite microstructure increases with a decrease in PAGS.
2. The critical temperature A_{c1} during heating is not affected by PAGS.

3. The nucleation sites for austenite formation are prior austenite grain boundaries for an initial martensite microstructure.
4. The mathematical modeling of the kinetics of austenite formation from an initial martensite microstructure was successfully conducted, where the model provided the amount of austenite formed for a given time, heating rate, and prior austenite grain size.

This study identified the importance of the initial grain size on the kinetics of austenite formation by providing a mathematical model of the martensite-to-austenite transformation. This research was conducted on two distinct prior austenite grain sizes, representative of the surface and core regions of large ingots. Subsequent studies could explore a more extensive range of PAGS. The findings of this result will help optimize the thermal processes of heat treatments of steels in the manufacturing industry.

Author Contributions: Conceptualization, N.R., H.C. and M.J.; methodology, N.R.; software, N.R. and M.S.; validation, N.R. and M.S.; formal analysis, N.R., M.S., H.C. and M.J.; investigation, N.R. and M.S.; writing—original draft, N.R.; writing—review and editing, M.S., P.B., H.C. and M.J.; supervision, P.B., H.C. and M.J.; project administration, H.C. and M.J.; funding acquisition, H.C. and M.J. All authors have read and agreed to the published version of the manuscript.

Funding: The authors express their gratitude to the Natural Sciences and Engineering Research Council of Canada (NSERC), the Metal Transformation Research and Innovation Consortium of Quebec (CRITM), Finkl Steel—Sorel, and Hydro-Québec Research Institute (IREQ) for supporting this research study through funding grant RDCPJ 515324–17.

Data Availability Statement: The original contributions presented in this study are included in the article. Further inquiries can be directed to the corresponding author.

Conflicts of Interest: The authors declare that they have no known competing financial interests or personal relationships that could have appeared to influence the work reported in this paper.

References

1. Celada-Casero, C.; Sietsma, J.; Santofimia, M.J. The role of the austenite grain size in the martensitic transformation in low carbon steels. *Mater. Des.* **2019**, *167*, 107625. [[CrossRef](#)]
2. Enomoto, M.; Hayashi, K. Modeling the growth of austenite in association with cementite during continuous heating in low-carbon martensite. *J. Mater. Sci.* **2018**, *53*, 6911–6921. [[CrossRef](#)]
3. Ben Fredj, E.; Nanesa, H.G.; Jahazi, M.; Morin, J.-B. Influence of initial microstructure and grain size on transformation of bainite to austenite in large size forgings. *J. Iron Steel Res. Int.* **2018**, *25*, 554–562. [[CrossRef](#)]
4. Dannoshita, H.; Ogawa, T.; Maruoka, K.; Ushioda, K. Effect of Initial Microstructures on Austenite Formation Behavior during Intercritical Annealing in Low-Carbon Steel. *J. Soc. Mater. Sci. Jpn.* **2019**, *68*, 718–722. [[CrossRef](#)]
5. Singh, J.; Wayman, C.M. Age-hardening characteristics of a martensitic Fe-Ni-Mn alloy. *Mater. Sci. Eng.* **1987**, *93*, 227. [[CrossRef](#)]
6. Wei, R.; Enomoto, M.; Hadian, R.; Zurob, H.; Purdy, G.R. Growth of austenite from as-quenched martensite during intercritical annealing in an Fe–0.1C–3Mn–1.5Si alloy. *Acta Mater.* **2013**, *61*, 697–707. [[CrossRef](#)]
7. Shinozaki, T.; Tomota, Y.; Fukino, T.; Suzuki, T. Microstructure Evolution during Reverse Transformation of Austenite from Tempered Martensite in Low Alloy Steel. *ISIJ Int.* **2017**, *57*, 533–539. [[CrossRef](#)]
8. Settini, A.G.; Chukin, D.; Pezzato, L.; Gennari, C.; Brunelli, K.; Dabalà, M. The impact of high heating rates on the austenitization process of 18NiCrMo5 steel. *Mater. Phys. Mech.* **2019**, *42*, 717. [[CrossRef](#)]
9. Mohsenzadeh, M.S.; Mazinani, M. The Influence of Microstructural Characteristics on Austenite Formation Kinetics in a Plain Carbon Steel. *Met. Mater. Trans. A* **2019**, *51*, 116–130. [[CrossRef](#)]
10. Wang, L.M.; Wang, Z.B.; Lu, K. Grain size effects on the austenitization process in a nanostructured ferritic steel. *Acta Mater.* **2011**, *59*, 3710–3719. [[CrossRef](#)]
11. De Andrés, C.G.; Caballero, F.; Capdevila, C.; Bhadeshia, H. Modelling of kinetics and dilatometric behavior of non-isothermal pearlite-to-austenite transformation in an eutectoid steel. *Scr. Mater.* **1998**, *39*, 791–796. [[CrossRef](#)]
12. Roósz, A.; Gácsi, Z.; Fuchs, E.G. Isothermal formation of austenite in eutectoid plain carbon steel. *Acta Met.* **1983**, *31*, 509–517. [[CrossRef](#)]

13. Oliveira, F.; Andrade, M.; Cota, A. Kinetics of austenite formation during continuous heating in a low carbon steel. *Mater. Charact.* **2006**, *58*, 256–261. [[CrossRef](#)]
14. López-Martínez, E.; Vázquez-Gómez, O.; Vergara-Hernández, H.J.; Campillo, B. Effect of initial microstructure on austenite formation kinetics in high-strength experimental microalloyed steels. *Int. J. Miner. Met. Mater.* **2015**, *22*, 1304–1312. [[CrossRef](#)]
15. Caballero, F.G.; Capdevila, C.; de Andrés, C.G. Kinetics and dilatometric behaviour of non-isothermal ferrite–austenite transformation. *Mater. Sci. Technol.* **2001**, *17*, 1114–1118. [[CrossRef](#)]
16. Ranjan, R.; Singh, S.B. Formation of austenite in steels during heating: Analysis of dilatation data. *Mater. Sci. Technol.* **2019**, *35*, 782–790. [[CrossRef](#)]
17. de Andrés, C.G.; Caballero, F.; Capdevila, C.; Martín, D.S. Revealing austenite grain boundaries by thermal etching: Advantages and disadvantages. *Mater. Charact.* **2003**, *49*, 121–127. [[CrossRef](#)]
18. Sadeghifar, M.; Sedaghati, R.; Jomaa, W.; Songmene, V. Finite element analysis and response surface method for robust multi-performance optimization of radial turning of hard 300M steel. *Int. J. Adv. Manuf. Technol.* **2017**, *94*, 2457–2474. [[CrossRef](#)]
19. *MATLAB® User Manual, R2020b*; The MathWorks, Inc.: Portola Valley, CA, USA, 2020.
20. Wang, W.; Wang, L.; Lyu, P. Kinetics of austenite growth and bainite transformation during reheating and cooling treatments of high strength microalloyed steel produced by sub-rapid solidification. *Int. J. Miner. Met. Mater.* **2022**, *30*, 354–364. [[CrossRef](#)]
21. Rezaei, J.; Parsa, M.H.; Mirzadeh, H. Phase transformation kinetics of high-carbon steel during continuous heating. *J. Mater. Res. Technol.* **2023**, *27*, 2524–2537. [[CrossRef](#)]
22. Ferreira, V.M.; Mecozzi, M.G.; Petrov, R.H.; Sietsma, J. Details of pearlite to austenite transformation in steel: Experiments and phase-field modeling. *Comput. Mater. Sci.* **2023**, *228*, 112368. [[CrossRef](#)]
23. Speich, G.R.; Demarest, V.A.; Miller, R.L. Formation of Austenite During Intercritical Annealing of Dual-Phase Steels. *Met. Trans. A* **1981**, *12*, 1419–1428. [[CrossRef](#)]
24. Speer, J.G.; Gaster, R.J. *Steel Heat Treating Fundamentals and Processes*; Dossett, J., Totten, G.E., Eds.; ASM International: Almere, The Netherlands, 2013; Volume 4, pp. 309–316. [[CrossRef](#)]
25. Cahn, J.W. The kinetics of grain boundary nucleated reactions. *Acta Met.* **1956**, *4*, 449–459. [[CrossRef](#)]
26. Christian, J.W. *The Theory of Transformations in Metals and Alloys*; Elsevier: Amsterdam, The Netherlands, 2002.
27. Shewmon, P. *Diffusion in Solids*; Springer: Cham, Switzerland, 2016. [[CrossRef](#)]

Disclaimer/Publisher’s Note: The statements, opinions and data contained in all publications are solely those of the individual author(s) and contributor(s) and not of MDPI and/or the editor(s). MDPI and/or the editor(s) disclaim responsibility for any injury to people or property resulting from any ideas, methods, instructions or products referred to in the content.